ARTIFICIAL SATELLITES, Vol. 48. No. 4 – 2013
DOI: 10.2478/arsa-2013-0015

EVALUATION OF SYMMETRIC NEUTRAL-ATMOSPHERE MAPPING FUNCTIONS USING RAY-TRACING THROUGH RADIOSONDE OBSERVATIONS

A.H. Souri, M.A. Sharifi
(souri_rs@ut.ac.ir, sharifi@ut.ac.ir)
Department of Surveying and Geomatics Engineering, University College of Engineering, University of Tehran, North Kargar Ave., P.O. Box 11365-4563, Tehran, Iran

Abstract.

The aim of this paper is to compare the validity of six recent symmetric mapping functions. The mapping function models the elevation angle dependence of the tropospheric delay. Niell Mapping Function (NMF), Vienna Mapping Function (VMF1), University of New Brunswick-VMF1 (UNB-VMF1) mapping functions, Global Mapping Function (GMF) and Global Pressure and Temperature (GPT2)/GMF are evaluated by using ray tracing through 25 radiosonde stations covering different climatic regions in one year. The ray-traced measurements are regarded as "ground truth". The ray-tracing approach is performed for diverse elevation angle starting at 5^o to 15^o. The results for both hydrostatic and non-hydrostatic components of mapping functions support the efficiency of online-mapping functions. The latitudinal dependence of standard deviation for 5^o is also demonstrated. Although all the tested mapping functions can provide satisfactory results when used for elevation angles above 15^o, for high precision geodetic measurements, it is highly recommended that the online-mapping functions (UNBs and VMF1) be used. The results suggest that UNB models, like VMF have strengths and weaknesses and do not stand out as being consistently better or worse than the VMF1. The GPT2/GMF provided better accuracy than GMF and NMF. Since all of them do not require site specific data; therefore GPT2/GMF can be useful as regards its ease of use.

Keywords: Mapping functions, Ray-tracing, Geodetic measurements, Neutral atmosphere

1. INTRODUCTION

Radiometric space geodesy systems such GPS, Very Long Baseline Interferometry (VLBI) and InSAR technique are complicated by Earth's troposphere. Since the effect of the troposphere on radiometric signals does not depend on frequency, dealing with the troposphere delay is problematic, requiring some models and techniques to mitigate it. Researchers have taken advantage of radiosonde observation in order to measure main atmosphere parameters having an impact on the delay (Mendez, 1999); in addition, Numerical Weather Models (NWM) provides 4-D (both space and time) state of atmosphere parameters that are an attractive source of data for tropospheric delay mitigation and climate monitoring. The common separation of the path delay is into a hydrostatic and non-hydrostatic (wet) (Davis et al., 1985). Since the hydrostatic delay is directly linked to total pressure, it can conveniently be removed by surface pressure at a site (Saastamoinen, 1973). Although there are a lot of models (e.g. Chao, 1971; Callahan, 1973; Berman, 1976; Baby et al., 1988) to relate some surface measurements to wet delay, no significant correlation was found (Mendez, 1999). However, it is feasible to estimate wet delay using a GPS station (PPP strategy) or a network solution; the delay is assumed constant for a given time interval; afterwards estimating its value as part of the overall least square inversion (the "deterministic" approach) (Bevis et al., 1992). The main condition that we should take into account is that the systems measure a path in out of zenith angle. The tropospheric delay is shortest in zenith direction and will become larger with increasing zenith angle. Projection of zenith path delays into slant direction is performed by application of a mapping function. The mapping functions that are independent of the azimuth of the observation have been calculated for the hydrostatic and the non-hydrostatic component separately by fitting coefficients of a continued fraction form (Marini, 1972) to ray-traced measurements performed through radiosonde data or numerical weather models. In the last decade, the recent mapping functions (both hydrostatic and non-hydrostatic) have not been separated clearly; the need of a new separation is required due to the way of use. The recent mapping function can be distributed mainly in two major groups. First, a group of mapping function is based on raytracing through monthly mean profiles or standard profiles including NMF (Niell, 1996), GMF (Boehm, J. et al., 2006a) and GPT2/GMF (Lagler et al., 2013). They do not need any additional data as an input. The second group is constituted by mapping function based on raytracing through Numerical Weather Models online, consisting of VMF1 (Boehm, J. et al., 2006b), UNB-CMC and UNB-NCEP (Marcelo C. Santos, 2012); therefore some information are needed to be downloaded. A wide variety of mapping function before 1996 has been tested by (Mendez, 1999). For both hydrostatic and non-hydrostatic mapping functions, it was concluded that NMF performed the best accuracy when compared to 32,467 ray-traced measurements through 50 radiosonde stations at diverse elevation angles. It is a common practice to evaluate the mapping functions in respect to station height parameter, since the delay is absorbed mainly by the height domain. VMF1 was compared to NMF in global GPS analysis and an average relative improvement (about 6%) was achieved (Boehm et al., 2007).

The next section represents a ray tracing method that was carried out to evaluate the performance of the mapping functions. Section two describes the used data that consist of 25 radiosonde measurements over entire globe and procedure for analyzing the mapping functions. Section three represents the results and finally, conclusion and recommendation are represented in the final section.

2. RAY TRACING

According to the American Meteorological Society's Glossary of Meteorology (AMS, 2007), ray tracing can be defined as:

"a graphical or mathematical approximation scheme for determining the propagation of electromagnetic or sound waves by following the path of rays obeying the laws of reflection and refraction."

In order to trace a ray in a direction other than zenith, one requires the slant distance that the ray travels in each layer of refractivity. Therefore with exact knowledge of refractivity profile along the whole ray path, the delay can be computed. In General, the propagation delay can be deduced from the 3-D Eikonal equation (Paris, D. T., and F. K. Hurd, 1969). In order to solve the Eikonal equation, three gradient components of the refractive index must be provided: $\frac{\partial n(r,\varphi,\lambda)}{\partial r}$, $\frac{\partial n(r,\varphi,\lambda)}{\partial \lambda}$ and $\frac{\partial n(r,\varphi,\lambda)}{\partial \varphi}$ (in spherical coordinate system (r,φ,λ)). The outputs of the partial differential equation are the coordinates of the points along the trajectory of the signal. Consequently by combining these coordinates and refractivity information, the total delay for our observation is measured. However based on the assumption of symmetric atmosphere (or horizontally stratified atmosphere, where $\frac{\partial n(r,\varphi,\lambda)}{\partial \lambda}, \frac{\partial n(r,\varphi,\lambda)}{\partial \varphi} = 0$) the Eikonal equation can be simplified to a horizontal stratified approximation model (Thayer, G. D., 1967). In this case, we assume that the ray does not leave the plane of constant azimuth. With this assumption we can also perform the highly simplified ray-tracing by continuously computing the refracted ray-pieces by following Snell's law called "Piece-Wise Linear Propagation" (Hobiger et al., 2008). According to (Hobiger et al., 2008) there is hardly difference between Thayer approximation and Piece-Wise Linear Propagation at 5^{o} elevation angle (less than 1mm), particularly for moderate to calm weather; consequently, in case of using radiosonde observations, which are 1-D measurements, it would be more practical to utilize the ray-pieces method.

In order to describe the ray-tracing system (Boehm, 2004) implemented in this work, we can distinguish three properties:

❖ Inputs:
- Radiosonde measurements providing basic metrological parameters in order to calculate the refractivity.
- Geographic coordinate of the stations (including altitude) and time of observation (typically modified Julian date in order to calculate the mentioned coefficient with reference date of Niell's calculations)
- Elevation angle
- Size of increments of interpolation

❖ Ray-tracing method

Assume that the hydrostatic and non-hydrostatic refractivities have been already determined from station elevation up to 100km. The distances from the center of Earth to an observation can be computed by:

$$r_i = r_0 + \sum_{i=1}^{k} h_i \quad (1)$$

Where h_i is the height of ith level and r_0 is the radius of the Earth that can be given by:

$$r_0 = \frac{a\sqrt{1-e}}{1-e^2 sin^2\varphi} \quad (2)$$

where *a* and *e* denote the semi major axis and the eccentricity of the WGS84 reference ellipsoid, respectively. For starting point, the initial elevation angle *e1* is known, according to figure1 we get:

$$\theta_1 = e_1 \quad (3)$$

The distance between first and second point can be measured with:

$$s_1 = -r_1 sin\theta_1 + \sqrt{r_2^2 - r_1^2 cos^2\theta_1} \quad (4)$$

The coordinates of P1 and P2 are:

$$z_1 = r_1 \quad (5) \qquad y_1 = 0 \quad (7)$$

$$z_2 = z_1 + s_1 sine_1 \quad (6) \qquad y_2 = y_1 + s_1 cose_1 \quad (8)$$

The corresponding angles at the geocenter are:

$$\eta_1 = 0 \tag{9}$$

$$\eta_2 = \arctan\left({}^{y_2}/_{z_2}\right) \tag{10}$$

by applying Snell's law the angles θ_2 and e2 at the point P2 can be computed:

$$\theta_2 = arccos\left(\frac{n_1}{n_2}\cos\left(\theta_1 + \eta_2\right)\right) \tag{11}$$

$$e_2 = \theta_2 - \eta_2 \tag{12}$$

For the next points we can measure all above parameters into a loop running from 2 to (k-1):

$$s_i = -r_i sin\theta_1 + \sqrt{r_{i+1}^2 - r_i^2 cos^2\theta_i} \tag{13}$$

$$z_{i+1} = z_i + s_i sine_i \quad (14) \qquad\qquad y_{i+1} = y_i + s_i cose_i \tag{15}$$

$$\eta_{i+1} = \arctan\left({}^{y_{i+1}}/_{z_{i+1}}\right) \tag{16}$$

$$\delta_{i+1} = \eta_{i+1} - \eta_i \tag{17}$$

$$\theta_{i+1} = arccos\left(\frac{n_i}{n_{i+1}}\cos\left(\theta_i + \delta_{i+1}\right)\right) \tag{18}$$

$$e_{i+1} = \theta_{i+1} - \eta_{i+1} \tag{19}$$

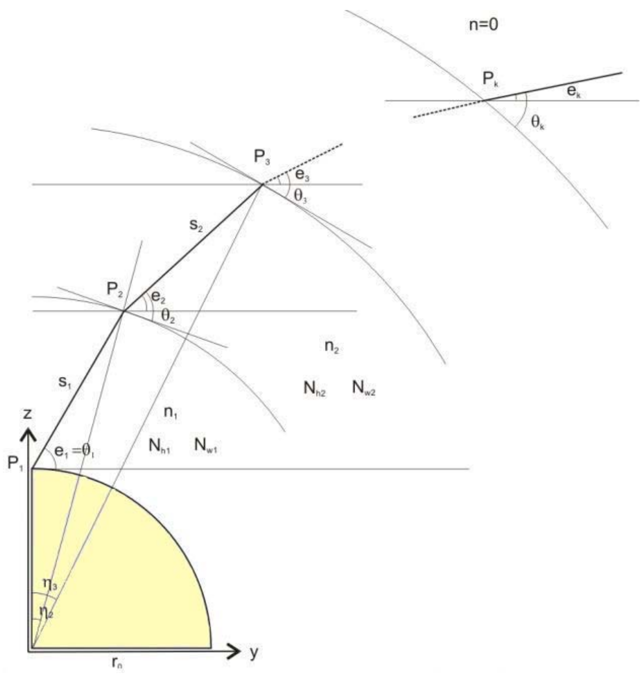

Figure 1. The schematic of the ray-tracing method (Boehm, 2004)

❖ Outputs

By using the equations above, all incremental distances s_i between the points and the final elevation angle called "outgoing elevation angle" are known. In the case of all geodetic techniques and mentioned mapping functions, the true elevation angle which is the angle between the radial vector local tangent plane and the straight line between the station and the source (satellite/radio) is used. Since the ray has been complicated by so-called "ray-bending effect", the outgoing elevation angle is not the same as the true elevation angle (see figure2). Therefore the initial elevation angle is needed to be increased a bit more and subsequently the outgoing elevation angle has to be compared to. This implies that any ray-tracing system should be iterated until a defined threshold is reached. A prior empirical model proposed by (Hobiger et al., 2008) is used in this work that its aim is reducing the number of iteration.

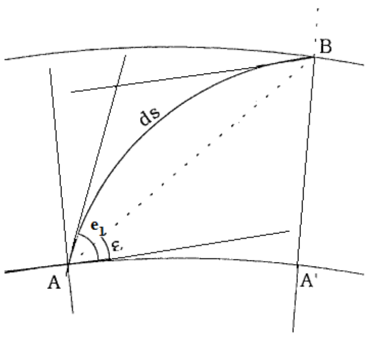

Figure 2. the difference between true elevation angle and intial elevation angle

The hydrostatic and non-hydrostatic delays along the bended ray can be measure by:

$$d_h = \sum_{i=1}^{k-1} s_i N_h \tag{20}$$

$$d_{nh} = \sum_{i=1}^{k-1} s_i N_{nh} \tag{21}$$

as mentioned before, the second term of the delay is geometric delay due to bending that can determined by:

$$d_{geo} = \sum_{i=1}^{k-1} (s_i - \cos(e_i - e_k) \times s_i) \tag{22}$$

The above term is usually added to the hydrostatic component.

3. METHODOLOGY AND USED DATA

The evaluation of the symmetric mapping functions by ray-traced measurements needs the Earth's atmosphere to be divided into series of thin concentric spherical shells, within which a constant refractivity is assumed. In order to obtain the refractivity profile, 25 radiosonde stations have been selected in this work. Radiosonde measures pressure, temperature and relative humidity from the surface up to typically 30km two times a day. Radiosonde instruments are produced by different manufactures and sensors; consequently they have different accuracy and top-height. As a result of magnificent improvement in sensors performance, the measurement errors maintained for modern radiosonde are usually small and have minimum accuracy as listed in (FMH, 1997):

Table1. The minimum accuracy of radiosonde observations (FMH, 1997).

Variable	**Accuracy**
Temperature	0.5° C
Relative Humidity	5%
Pressure	1.0 hPa (P>300 hPa) 1.5 hPa (50 hPa<P≤ 300 hPa) 1.0 hPa (P ≤ 50 hPa)

It is necessary to determine how sensitive Zenith Hydrostatic Delay (ZHD) and Zenith Wet Delay (ZWD) are to errors in the value of radiosonde measurements. Sensitivity may then be measured by monitoring errors in the outputs which means by partial derivatives and applying the error propagation law (with neglecting correlation among parameters).

There are three steps for obtaining the refractivity shells from radiosonde measurements: firstly, the relative humidity must be converted to water vapor pressure that is an input for the determination of refractivity; secondly, each profile has to be interpolated between the measured levels by the instrument and extrapolated beyond the last observed height. The final step is the calculation of both hydrostatic and non-hydrostatic components of refractivity. In order to convert the relative humidity to water vapor pressure, the following equation can be used (Mendez, 1999):

$$e = e'_{sw}\frac{U}{100}\left[1-\left(1-\frac{U}{100}\right)\frac{e'_{sw}}{P}\right]^{-1} \tag{23}$$

Where U is the relative humidity, P is the total pressure and e'_{sw} is the saturation vapor pressure of moist air.

In fact, the saturation pressure of water vapor in moist air is not same as the saturation pressure of pure water vapor. The ratio of saturation vapor pressure of moist air to that pure water is called the enhancement factor, f_w. For high-accuracy application, a model is used (Buck, A.L, 1981). Therefore the saturation vapor pressure of moist air can be obtained by:

$$e'_{sw} = e_{sw}f_w \tag{24}$$

In order to compute the saturation vapor pressure over both surface of water and ice, a large selection of formulae is available. In (Mendez, 1999), The Wexler formula has been proved the most accurate generic model. The temperature and relative humidity for each layer can be linearly interpolated within an initial step size (e.g. 5 m). Regarding the fact that pressure decreases exponentially with height, the logarithm-transformed pressure values were interpolated linearly. For extrapolation of temperature profile, U.S Standard atmosphere was used and for total pressure, isothermal assumption of atmosphere was considered. The profiles were extrapolated from the last altitude to 100km. As mentioned before, the relative humidity in high altitudes (e.g. 30km) is negligible. Therefore there is no need for performing extrapolation of humidity. The number of shells or the step size should be adequately small to prevent abnormal variations of the refractivity compared to wavelength. Although small step sizes leads to better accuracy, the computation time will be significantly increased. Nevertheless, we do not care about the computation time; consequently the step size is set to 1 meter in this work. After the determination of profiles, the hydrostatic and non-hydrostatic component of refractivity can be computed. For an example, the both components have been determined for PHTO radiosonde station in Hawaii on 12/22/2012 at 12:00 UT:

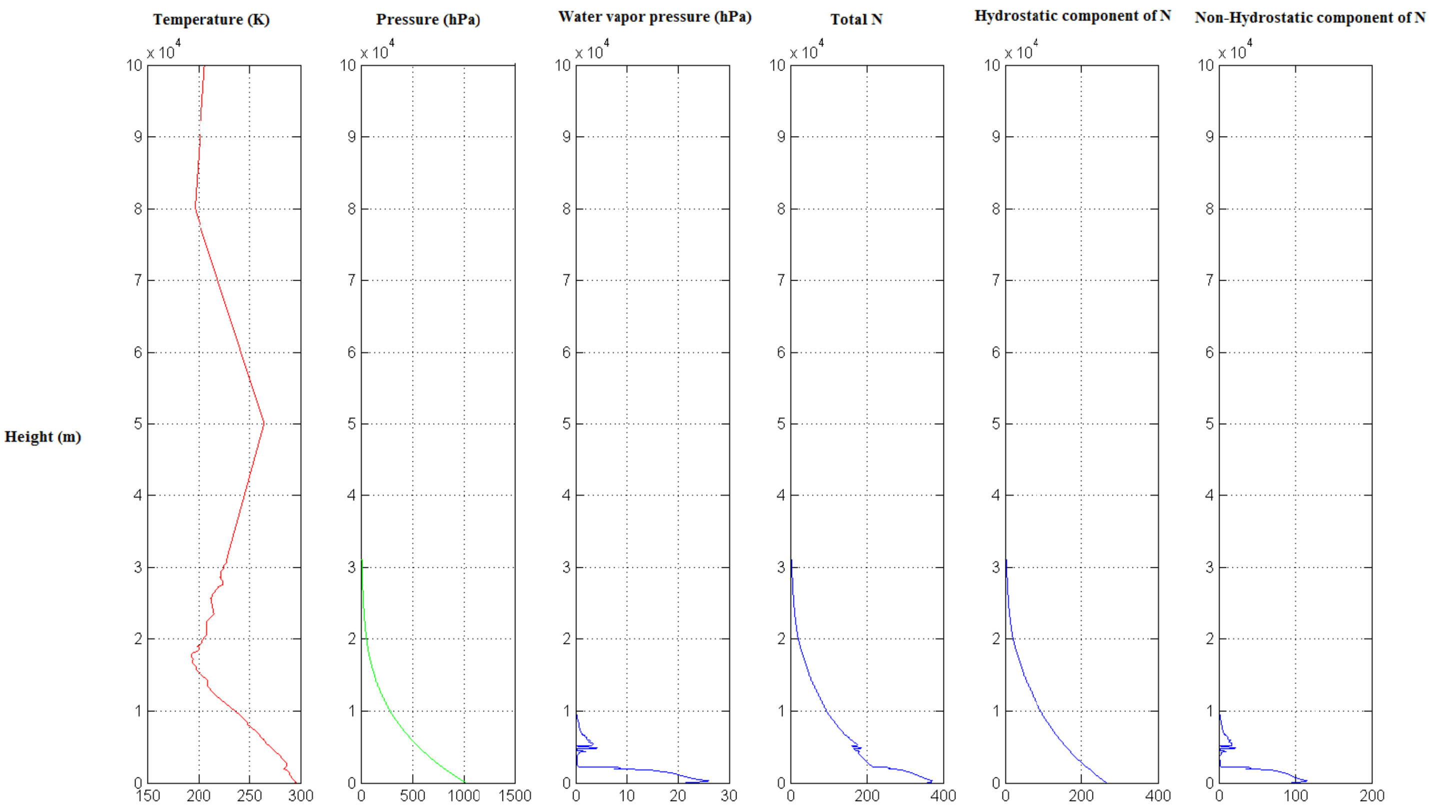

Figure 3. The profiles and neutral-atmosphere refractivity retrieved by radiosonde (PHTO station)

As mentioned before, 20 radiosonde stations were chosen for ray tracing purposes. The ray tracing method was performed at six elevation angles: 5^o, 7.5^o,10^o,15^o ,90^o. Because radiosonde measures the profiles nominally two times in one day, for each elevation angle, 14,600 traces were produced for a year of measurements. The ray traced zenith delay was assumed the quantity to be mapped for each mapping function and the propagation delays generated by ray tracing were assumed errorless. The accuracy of a mapping function can be evaluated in terms of bias(δ), standard deviation(σ) and total error(γ). The bias is the difference of the values given by the mapping function and the ray-traced values. In order to rank the mapping functions, the total error is defined as:

$$\gamma = \sqrt{\delta^2 + \sigma^2} \tag{25}$$

The mapping functions errors (particulary standrad deviation) can be compared in different latitudes; therefore the latituidal dependence of the error will be investigated.

The investigation of water vapor variability is needed to be done in order to interpret the latitudinal dependence of the non-hydrostatic errors. Precipitation Water Vapor (PWV) is one of the key parameters for the analysis of global climate systems, formation of clouds and short-term forecasts of precipitation. It is directly linked to Integration Water Vapor (IWV) and subsequently ZWD. The NASA Water Vapor Dataset-M (NVAP-M) provided gridded PWV and layered water vapor avaiable over both land and ocean (NVAP-M ATBD, 2013) . It has three separate products directed to towards specific research goal. The NVAP-M Climate which is ideal for studies of interannual variability and climate is used. The product dataset was constructed using data from SSM/I intercalibarated, High Resolution Infrared Sounder (HIRS), radiosonde retrievals and Atmospheric Infrared Sounder (AIRS). The product is available at $1^{o} \times 1^{o}$ resolution at daily temporal resolution between 2001 and 2009 (Website1). Annual mean and standard deviation of PWV using every ten days data in 2007 are calculated (figure4). Both mean and standard deviation are improtant to identify the most variable regions with high amplitudes; accordingly a map is produced by multiplying annual standard deviation to mean (figure 5).

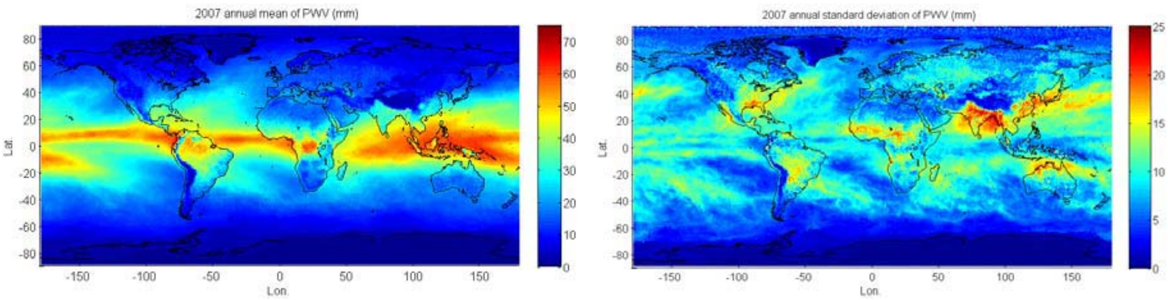

Figure 4. Left: annual mean of PWV in 2007; right: annual standard deviation of PWV in 2007

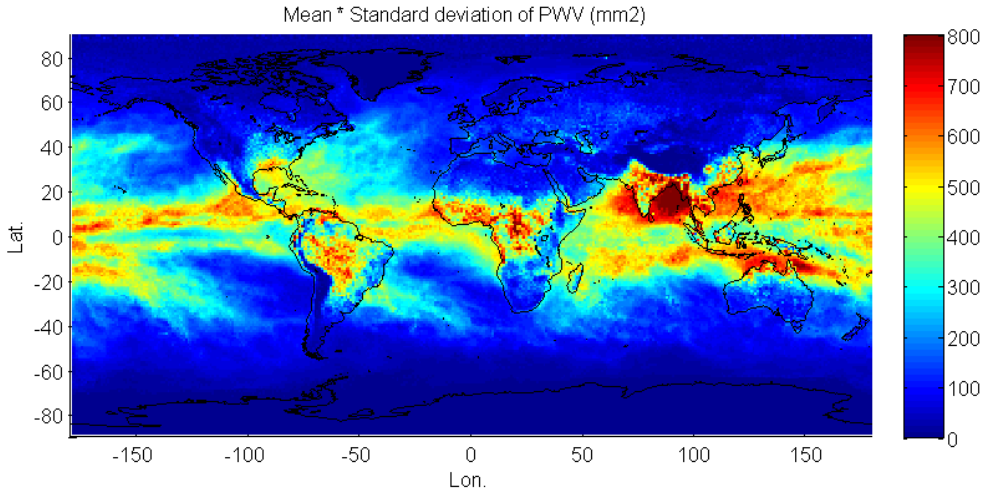

Figure 5. Mean × standard deviation of PWV in 2007.

4. RESULTS AND DISCUSSION

There have been number of investigations on radiosonde error on zenith delay and the proficiency of mentioned mapping function using ray-tarced measurments. Using propogation error law and radiosonde accuracy listed in table1, the effect of radiosonde error on both ZHD and ZWD are calculated at Davenport station, located along the Mississippi River (figure 6) for one-year observartion. The propogated errors of ZWD increase when the delay is great, particularly in summer when water vapor is expected to have high values. No such condition can be seen in ZHD. Both errors may only have sub-milimeters level effect on both ZHD and ZWD, although it can change for different locations. The results show that ray-traying through radiosonde measurements is satisfactorily reliable.

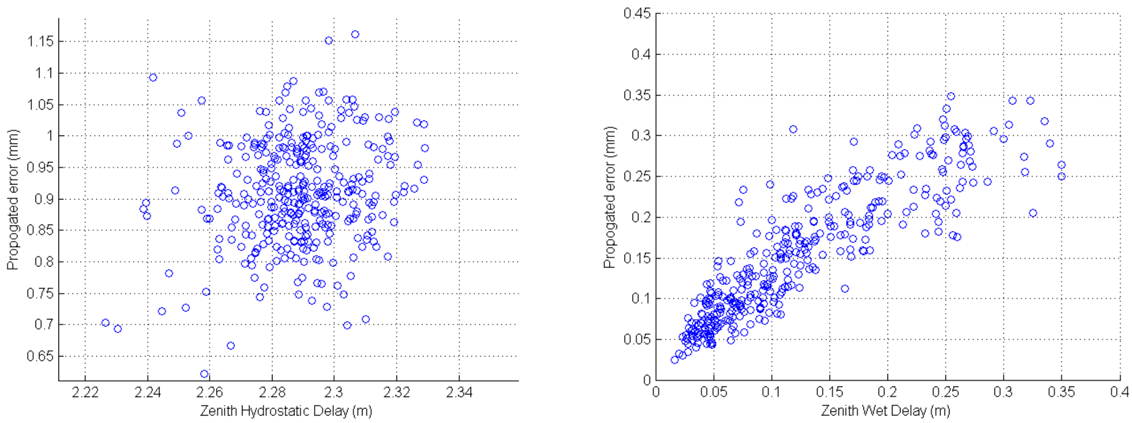

Figure 6. Left: propogated error of ZHD; right: propogated error of ZWD at Davenport station in one-year observation.

Since the mapping functions have been separated to hydrostatic and non-hydrostatic component, the analysis follows the same separation. The mapping functions accuracy in lower elevation angle is more distinguishable; therefore only the bias and standard deviation of the differences at 5^o elevation angle for hydrostatic component are listed:

Table 2. The bias for hydrostatic component at 5^o

Station	Country	Latitude	Longitude	Height(m)	NMF	GMF	GPT2/GMF	VMF	UNB-CMC	UNB-NCEP
89664	Antarctica	-77.85	166	24	31.1	18.5	14.3	8.5	8.8	8.4
89512	Antarctica	-75.5	333.35	30	23.6	10.6	10.7	7.6	7.4	7.2
89571	Antarctica	-68.58	77.96	22	26.8	22.2	23.3	10.5	10.8	9.8
89592	Antarctica	-66.55	93.01	40	20.2	25.5	24.6	11.2	12.1	11.5
89611	Antarctica	-66.28	110.53	42	25.4	26.1	22.4	6.9	7.1	7
EGYP	Falkland island	-51.81	301.55	73	17.5	5.2	6.7	5.8	6.5	6.1
YMHB	Australia	-42.83	147.5	27	-11.1	-3.3	-2.9	-3.5	-2.6	-4.2
YMML	Australia	-37.66	144.85	119	-3.4	-3.6	-3.2	-3.2	-3.1	-3.3
SAME	Argentina	-32.83	291.22	704	3.9	3	3.7	3.7	3.7	3.8
FABL	South Africa	-29.1	26.3	1354	-2.2	-2.5	-2	-2.4	-2.3	-2
FMSD	Haiti	-25.03	46.95	9	2.1	1.9	1.8	1.8	1.9	1.8
SBBR	Brazil	-15.86	312.07	1061	-1.8	-1.2	-1	-0.9	-1	-1.1
SBVV	Brazil	2.83	299.3	140	-2	-2.1	-2.1	-2	-1.9	-2
PHTO	Hawaii	19.71	204.94	11	0.3	0.2	-0.7	0.4	-0.9	-0.7
MMMD	Mexico	20.98	270.35	11	-2.7	-3.1	-3.4	-3	-2.8	-3
VIDD	India	28.58	77.2	216	-5.2	-4.8	-3.2	-3.3	-3.3	-3.9
DVN	USA- Iowa	41.61	269.42	229	-1.6	-1	-0.8	-0.4	-1	-1.1
RIW	USA- Wyoming	43.06	251.52	1703	-2.3	-2.9	-2.4	-2.1	-2.3	-2
ETGB	Germany	52.81	9.93	69	-1.2	-1.2	-1.6	-1.1	-1.4	-1.3
WSE	Canada-Alberta	53.53	245.9	766	4.5	4.3	4.2	4.2	4.2	4.3
YVP	Canada-Quebec	58.11	291.59	60	-2.2	0.8	0.8	0.7	0.8	1
ENOL	Norway	63.7	9.6	10	-6.8	-6.4	-6.2	-6	-6.5	-6.1
YEV	Canada-Inuvik	68.31	226.47	103	1.7	2.1	1.6	1.9	2	2.1
YRB	Canada-Nunavut	74.7	265.04	40	-6.7	-5.1	-5.4	-5.1	-4.8	-5
WLT	Canada-Nunavut	82.5	297.6	65	-9.3	-4.9	-4.2	-4.3	-4.4	-5

Table 3. The standard deviation for hydrostatic component at 5^o

Station	Country	Latitude	Longitude	Height(m)	NMF	GMF	GPT2/GMF	VMF	UNB-CMC	UNB-NCEP
89664	Antarctica	-77.85	166	24	50.5	44.2	44.6	40.7	40.4	41.5
89512	Antarctica	-75.5	333.35	30	46.1	43.6	41.8	38.2	38.3	39
89571	Antarctica	-68.58	77.96	22	45.5	44.5	44.9	42.6	42.7	43.1
89592	Antarctica	-66.55	93.01	40	43.8	42.5	44.1	40.5	40.2	40.9
89611	Antarctica	-66.28	110.53	42	42.6	43.4	38.2	35.1	35.5	37
EGYP	Falkland island	-51.81	301.55	73	39.3	37.8	37.3	34.7	34.8	34.5
YMHB	Australia	-42.83	147.5	27	38.1	38.7	37.9	33.5	32.9	33.6
YMML	Australia	-37.66	144.85	119	37.1	36.8	36.2	34.2	34.2	34
SAME	Argentina	-32.83	291.22	704	37.2	36.4	37	32.9	33	33
FABL	South Africa	-29.1	26.3	1354	34.6	33.1	33.9	33.8	33.8	33.4
FMSD	Haiti	-25.03	46.95	9	32.9	32.1	32.9	31.1	31	31.2
SBBR	Brazil	-15.86	312.07	1061	29.9	29.8	29.8	28.9	28.4	29
SBVV	Brazil	2.83	299.3	140	27.1	27.2	27.2	27.2	27.2	27.3
PHTO	Hawaii	19.71	204.94	11	30.6	30.5	29.8	29.4	29.1	29.3
MMMD	Mexico	20.98	270.35	11	32.2	32.4	32.3	31.6	32.1	31.4
VIDD	India	28.58	77.2	216	33.7	32.9	32.2	30.9	31	31.1
DVN	USA- Iowa	41.61	269.42	229	33.5	33.2	33.1	31.5	32.2	31.2
RIW	USA- Wyoming	43.06	251.52	1703	36.7	33.7	36.8	33.1	33	34
ETGB	Germany	52.81	9.93	69	35.8	35.9	35.1	32.7	32.8	32.7
WSE	Canada-Alberta	53.53	245.9	766	36.1	36	36	32.7	32.6	32.8
YVP	Canada-Quebec	58.11	291.59	60	37.4	36.4	36.2	33.1	33.2	33.1
ENOL	Norway	63.7	9.6	10	41.5	40.8	39.4	36.9	40.2	36.5
YEV	Canada- Inuvik	68.31	226.47	103	47.1	45.9	45.7	37.9	37.2	38.2
YRB	Canada-Nunavut	74.7	265.04	40	47	46.5	45.3	41.2	41.4	42.2
WLT	Canada-Nunavut	82.5	297.6	65	49.1	47.8	46.7	41.8	41.7	43.3

Although the mapping functions biases are approximately in consistent well with the radiosonde and with each other, the standard deviation obviously increases in high latitude regions. Since the most prominent pressure deviations are associated with the high latitude regions specifically, Arctic and Polar, which are the regions of most intensive cyclonic activity, the seasonal and monthly generic models are not able to simulate those high frequency variations. Consequently, the mapping functions that only depend on day of the year and station coordinate have greater standard deviation in high latitudes (see figure 7).

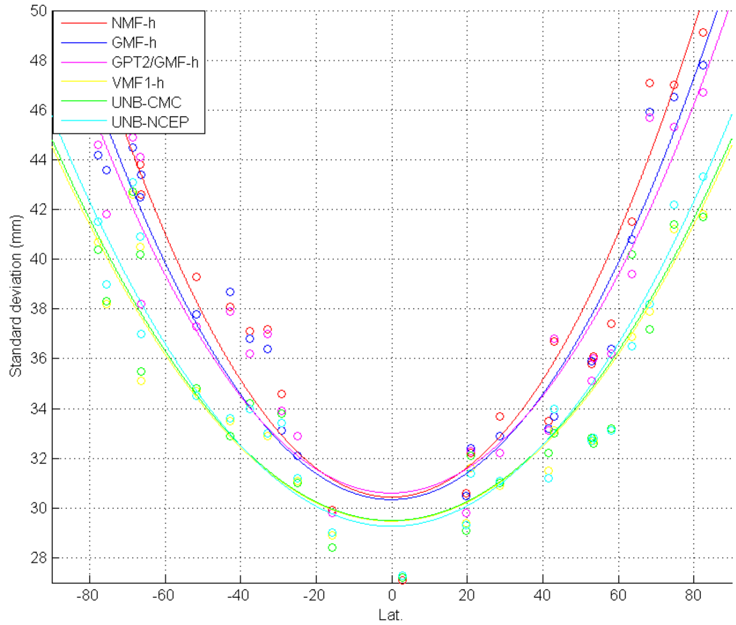

Figure 7. Standard deviation scatter for 5^{o} elevation angle due to hydrostatic component.

In order to evaluate which mapping function has better accuracy, a series of graphs will be depicted. The graphs are total error bar plot at four different elevation angles in mm. Hydrostatic component of the mapping function have been analyzed and the related total error, at four different elevation angles are represented in figure 8:

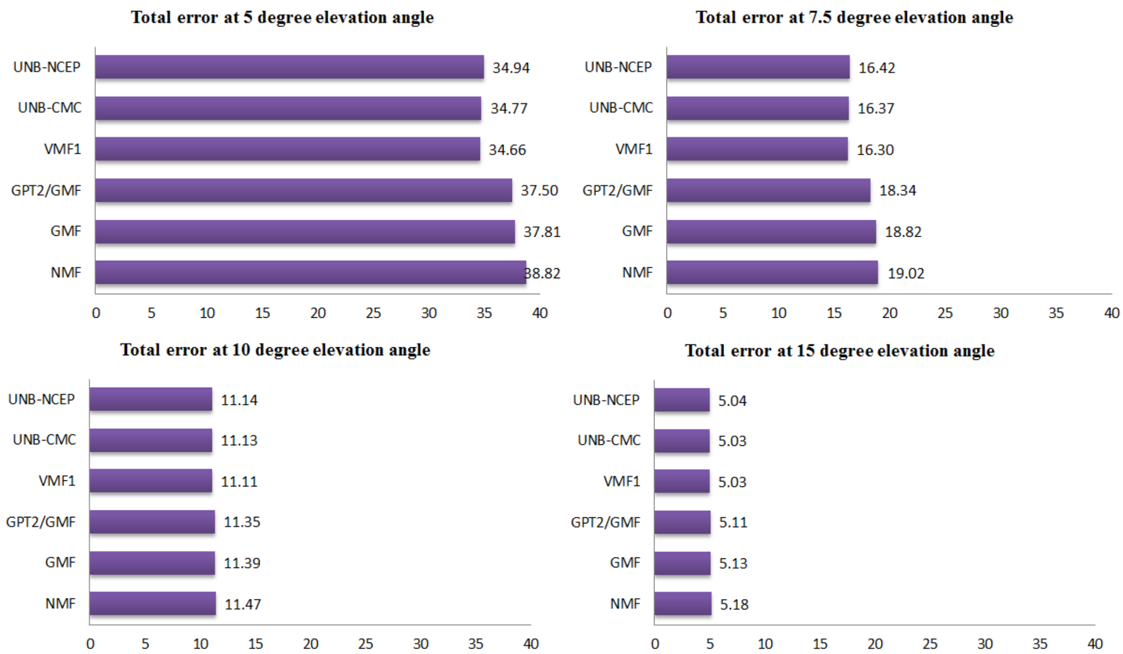

Figure 8. total error for hydrostatic component of the mapping functions as four different elevation angles (mm).

The figure shows the total error of the mapping functions in high elevation angle is very small (0.2% in respect to nominal zenith error: 2.3m); however by decreasing the elevation angle, the differences will be highlighted. At any elevation angles, VMF1 shows the best accuracy (1.5% at 5 elevation angle). If we merely consider NMF, GMF and GPT2/GMF which require no extra data, we can conclude that GPT2/GMF is the best independent on-line data for mapping hydrostatic component. The first reason for this result is that NMF used mean values of the North America however was applied over entire globe. Therefore local assumption of NMF could not be valid for the globe. The second reason is that spherical harmonic model used in the GMF and modification considered in GPT2 are able to model hydrostatic variation more efficiently than a simple sinusoidal model. Therefore, as regards the ease of use, GPT2/GMF is the best choice. There is hardly any difference between online mapping functions; each of them outperforms others' accuracy in different locations.

Non-hydrostatic component of the mapping functions have been computed and the related biases and standard deviations, at 5^o elevation angles are represented in table 4 and table 5:

Table4. The bias for non-hydrostatic component at 5^o

Station	Country	Latitude	Longitude	Height(m)	NMF	GMF	GPT2/GMF	VMF	UNB-CMC	UNB-NCEP
89664	Antarctica	-77.85	166	24	0.08	0.08	0.09	0.01	0.01	0.02
89512	Antarctica	-75.5	333.35	30	0.05	0.07	0.08	0.02	0.01	0.01
89571	Antarctica	-68.58	77.96	22	0.07	0.04	0.03	0.01	0.02	0.01
89592	Antarctica	-66.55	93.01	40	0.06	0.02	0.07	0.02	0.04	0.04
89611	Antarctica	-66.28	110.53	42	0.02	0.09	0.05	0.04	0.02	0.03
EGYP	Falkland island	-51.81	301.55	73	0.16	0.02	0.08	0.11	0.09	0.11
YMHB	Australia	-42.83	147.5	27	-0.07	-0.06	-0.08	-0.06	-0.08	-0.06
YMML	Australia	-37.66	144.85	119	-0.12	-0.13	-0.15	-0.12	-0.14	-0.11
SAME	Argentina	-32.83	291.22	704	0.09	0.1	0.07	0.07	0.07	0.08
FABL	South Africa	-29.1	26.3	1354	0.16	0.15	0.08	0.15	0.1	0.16
FMSD	Haiti	-25.03	46.95	9	0.05	0.09	0	0.02	0.01	0.03
SBBR	Brazil	-15.86	312.07	1061	-0.11	-0.17	-0.09	-0.1	-0.08	-0.1
SBVV	Brazil	2.83	299.3	140	0.35	0.18	0.13	0.15	0.14	0.15
PHTO	Hawaii	19.71	204.94	11	0.16	0.19	0.08	0.03	0.1	0.04
MMMD	Mexico	20.98	270.35	11	0.48	0.75	0.35	0.34	0.36	0.34
VIDD	India	28.58	77.2	216	-0.1	-0.09	-0.14	-0.09	-0.14	-0.08
DVN	USA- Iowa	41.61	269.42	229	0	0.2	0.7	0.1	0.71	0.1
RIW	USA- Wyoming	43.06	251.52	1703	0.2	0.3	0.2	0.2	0.21	0.2
ETGB	Germany	52.81	9.93	69	-0.12	0.12	0.16	0.11	0.16	0.11
WSE	Canada-Alberta	53.53	245.9	766	1.5	0.9	0.87	1	0.87	1
YVP	Canada-Quebec	58.11	291.59	60	0.08	0.18	0.16	0.16	0.18	0.17
ENOL	Norway	63.7	9.6	10	-0.3	-0.18	-0.23	-0.14	-0.21	-0.14
YEV	Canada- Inuvik	68.31	226.47	103	0.7	0.3	0.2	0.2	0.21	0.21
YRB	Canada-Nunavut	74.7	265.04	40	0.09	0.07	0.04	0.04	0.06	0.05
WLT	Canada-Nunavut	82.5	297.6	65	0.06	0.18	0.05	0.09	0.06	0.1

Table 5. The standard deviation for non-hydrostatic component at 5^o

Station	Country	Latitude	Longitude	Height(m)	NMF	GMF	GPT2/GMF	VMF	UNB-CMC	UNB-NCEP
89664	Antarctica	-77.85	166	24	9	9	8.9	8.9	9	9
89512	Antarctica	-75.5	333.35	30	9.1	9.3	9.2	9	9	8.9
89571	Antarctica	-68.58	77.96	22	9.9	10	9.5	9.7	9.4	9.7
89592	Antarctica	-66.55	93.01	40	10.1	10	10.1	9.8	10	9.8
89611	Antarctica	-66.28	110.53	42	10	9.9	9.7	9.8	9.7	9.9
EGYP	Falkland island	-51.81	301.55	73	10.8	10.5	10.5	10.5	10.5	10.4
YMHB	Australia	-42.83	147.5	27	11.2	10.9	10.1	9.4	9.3	9.3
YMML	Australia	-37.66	144.85	119	11.3	11	10.8	10	9.9	9.9
SAME	Argentina	-32.83	291.22	704	12.9	11.5	11.9	10.8	10.7	10.7
FABL	South Africa	-29.1	26.3	1354	11.3	10.9	10.2	10.2	10.2	10.1
FMSD	Haiti	-25.03	46.95	9	13	13.1	12.3	11.3	11.2	11.2
SBBR	Brazil	-15.86	312.07	1061	13.7	13	13.4	12.7	12.8	12.8
SBVV	Brazil	2.83	299.3	140	15.2	15.2	14.7	13.3	13.3	14.1
PHTO	Hawaii	19.71	204.94	11	13.4	12.7	12.3	11.6	11.6	12.1
MMMD	Mexico	20.98	270.35	11	12.6	11.9	11.6	10.9	10.9	11.2
VIDD	India	28.58	77.2	216	12.3	12.3	11.3	11.6	11.6	11.5
DVN	USA- Iowa	41.61	269.42	229	10.2	10.2	10.1	10	10.1	10.2
RIW	USA- Wyoming	43.06	251.52	1703	11.2	11.2	11.8	11.3	11.2	11.1
ETGB	Germany	52.81	9.93	69	11.4	10.8	11.2	10.7	10.6	10.6
WSE	Canada-Alberta	53.53	245.9	766	10.8	10.8	11	10.4	10.3	10.3
YVP	Canada-Quebec	58.11	291.59	60	10.4	10.1	9.7	10.6	10.5	10.5
ENOL	Norway	63.7	9.6	10	9.6	9.7	9.7	9.7	9.7	9.7
YEV	Canada- Inuvik	68.31	226.47	103	10.1	9.5	10.1	9.8	9.7	9.6
YRB	Canada-Nunavut	74.7	265.04	40	9.4	9.8	9.4	9.3	9.3	9.2
WLT	Canada-Nunavut	82.5	297.6	65	9.1	9	9	9.1	9	9

The plot at the left of figure4 demonstrates that the annually averaged maximum PWV occures just north of the equator. The maximum PWV values concentrates just north of the equator are called the Intertropical Convergence Zone (ITCZ) and the southest of the west Pacific warm pool is called the South Pacific Convergence Zone (SPCZ). The lowest values can be found in the high latitdes. Both magnitude of PWV and its variation (i.e. standard deviation) play an important role to interpret the latitudinal dependence of non-hydrostatic error. According to figure 5, the great variations of non-hydrosatic standard deviation would be expected in just near of equator. This is in coincinent with resultant standard deviation retrived from ray-traced measurments (see figure 9).

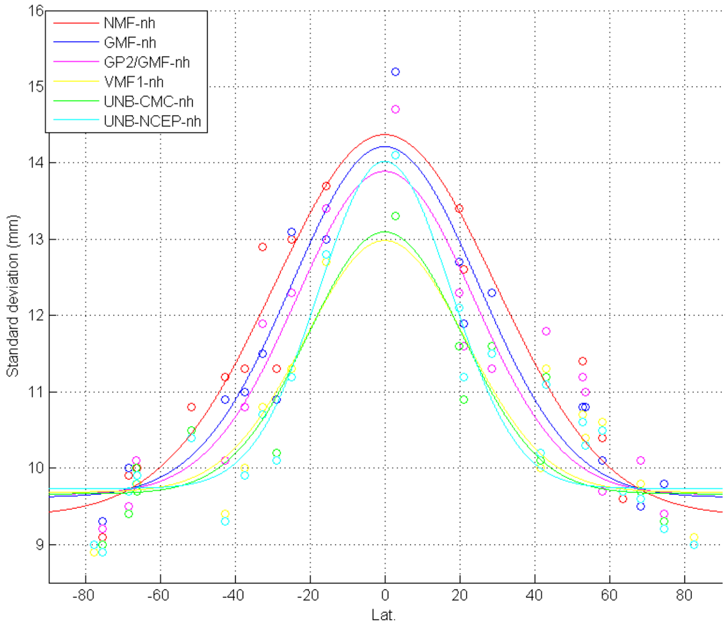

Figure 9. Standard deviation scatter for 5^{o} elevation angle due to non-hydrostatic component.

Non-hydrostatic component of the mapping function have been analyzed and the related total error, at four different elevation angles are represented in figure 10:

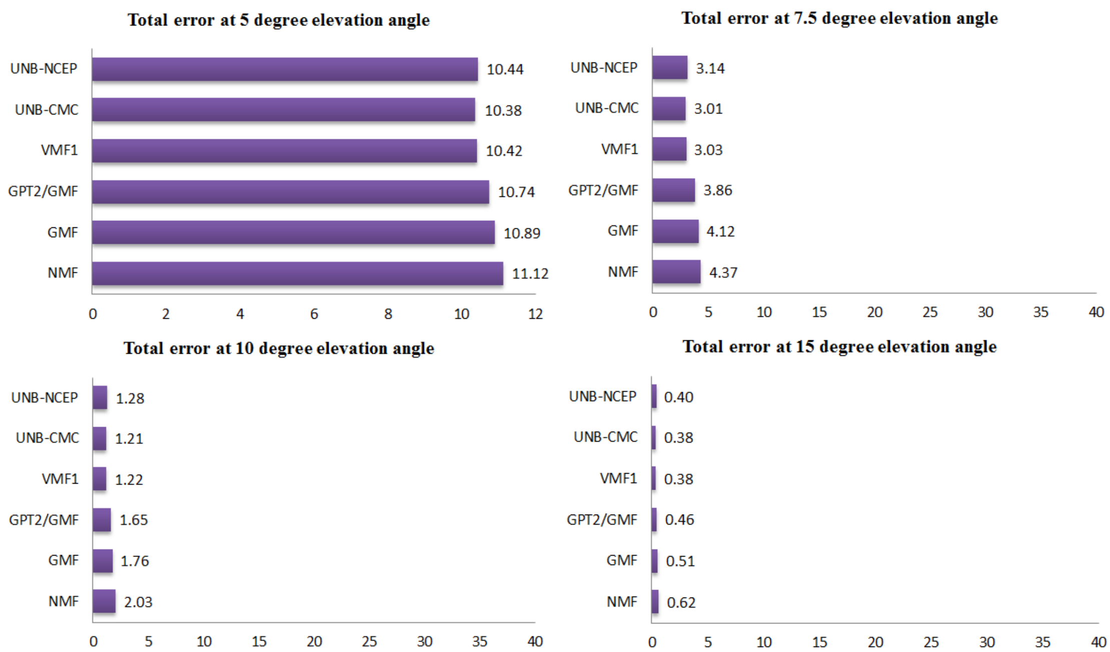

Figure 10. total error for non-hydrostatic component of the mapping functions as four different elevation angles (mm).

The results for non-hydrostatic components also supports the efficiency of online mapping functions; particularly, UNB-CMC shows only 4% error in respect to nominal zenith delay (25 cm) at 5^{o} elevation angle.

5. CONCLUSION

Based on the comparisons of six recent mapping functions and ray-traced measurements through 25 radiosonde stations, a number of conclusions can be drawn. Firstly, NMF is outdated because it has high total error at low elevation angles by relative to the GMF and GPT2/GMF that also do not require site specific data. Secondly, the NMF deficiency may be due to the fact that its functional formulation is only based on U.S. standard atmosphere data. Thirdly, GPT2 has been shown to improve upon the original atmospheric model used for the GMF. Although all the tested mapping functions can provide satisfactory results when used for elevation angles above 15, for high precision geodetic measurements, it is highly recommended that the on-line mapping functions be used. In general, the results indicate that the agreement of the UNBs models with the bias and standard deviation is not consistently better or worse than that of the VMF1. As seen before, the performance of any proposed mapping function strongly depends on which Numerical Weather Model (NWM) is used. Therefore introducing and analyzing coming mapping functions could be developed with further studies including: 1) utilizing new NWM with high spatial resolution for measuring new coefficients; 2) evaluation of mapping function by using InSAR technique aimed by cone reflector with known precise coordinate; 3) assessment of other regression formula in order to model the time variations of the coefficients.

Acknowledgements

We would like to thank Johannes Boehm and Virgilio Mendez for their support and giving us valuable advice for implementing ray-tracing method.

REFERENCES

AGU, December 1995: Water vapor in the climate system special report: http://www.eso.org/gen-fac/pubs/astclim/espas/pwv/mockler.html

AMS, 2007: Glossary of Meteorology. American Meteorological Society. On-line at http://amsglossary.allenpress.com/glossary

Baby, H. B., P. Gole, and J. Lavergnat, 1988: A model for the tropospheric excess path length of radio waves from surface meteorological measurements. Radio Science, Vol.23, No.6, pp. 1023-1038.

Bean, B.R. and E.J.Dutton, 1996: Radio Meteorology. National Burea of Standards Monograph 92, U.S Goverment Printing Office: Washington, D.C.

Berman, A.L., 1976: The prediction of zenith range refraction from surface measurements of meteorological parameters. JPL Technical Report 32-1602, Jet Propulsion Laboratory, California Institute of Technology, Pasadena, Calif.

Boehm Johannes, 2004: Troposphärische Laufzeitverzögerungen in der VLBI, Ph.D dissertation, The Institutes of the Course on 'Geodesy and Geoinformation' of the Vienna University of Technology.

Boehm, J., A. E. Niell, P. Tregoning, and H. Schuh, 2006a: Global Mapping Function(GMF): A new empirical mapping function based on numerical weather model data. Geophysical Research Letters, Vol. 33, No. L07304, doi:10.1029/2005GL025546.

Boehm, J., B. Werl, and H. Schuh, 2006b: Troposphere mapping functions for GPS and very long baseline interferometry from European Centre for Medium-Range Weather Forecasts operational analysis data. Journal of Geophysical Research, Vol. 111, No.B02406

Boehm, J., P.J. Mendes Cerveira, H. Schuh, P. Tregoning, 2007: The impact of mapping functions for the neutral atmosphere based on numerical weather models in GPS data analysis, IAG Symopsium Series, P. Tregoning and C. Rizos (Eds), pp. 837-843.

Buck, Al.L, (1981): New equations for computing vapor pressure and enhancement factor. Journal of applied meteorology, Vol.20, pp. 1527-1532.

Callahan, P.S., 1973: Prediction of tropospheric wet-component range error from surface measurements. Jet Propulsion Laboratory, California Institute of Technology, Pasadena, Calif., JPL Technical Report 32-1526, Vol. XVIII, pp. 41-46.

Chao, C.C., 1971: New tropospheric range corrections with seasonal adjustment. Jet Propulsion Laboratory, California Institute of Technology, Pasadena, Calif., JPL Technical Report 32-1526, Vol. VI, pp. 67-82.

Davis, J.L., T.A.Herring, I.I.Shapiro, A.E.E. Rogers and G.Elgered, (1985): Geodesy by radio interferometry: Effects of atmospheric modeling errors on estimated of baseline length. Radio science, Vol.20, No. 6,pp. 1593-1607.

Emardson, T. R., G. Elgered, and J. M. Johansson, 1998: Three months of continuous monitoring of atmospheric water vapor with a network of Global Positioning System receivers. J. Geophys. Res., Vol.103, pp. 1807– 1820

FMH, 1997: Federal Meteorological Handbook, No.3. Office of the Federal Coordinator for Meteorological Services and Supporting Research. Washington DC.

Hobiger, T., R. Ichikawa, Y. Koyama, and T. Kondo, 2008: Fast and accurate ray-tracing algorithms for real-time space geodetic applications using numerical weather models. J. Geophys. Res., 113, D20302, doi:10.1029/2008JD010503.

K. Lagler, M. Schindelegger,J. Böhm, H. Krásná,and T.Nilsson, 2013: GPT2: Empirical slant delay model for radio space geodetic techniques, Geophysical Research Letters, Vol. 40, pp. 1069–1073, doi:10.1002/grl.50288, 2013

Marcelo C. Santos, Matthew McAdam, and Johannes Boehm, 2012: Implementation Status of the UNB-VMF1, EGU General Assembly 2012 Vienna, Austria, pp. 22- 27.

Marini, J. W. 1972: Correction of satellite tracking data for an arbitrary tropospheric profile, Radio Science, Vol. 7, No. 2, pp. 223–231, doi:10.1029/RS007i002p00223.

Mendes, V.B. 1999: Modeling The Neutral-Atmosphere Propagation Delay in Radiometric Space Techniques. Ph.D. dissertation, Department of Geodesy and Geomatics Engineering Technical Report No. 199, University of New Brunswick, Canada.

Michael Bevis, Steven Businger, Thomas A. Herring, Christain Rocken, Richard A. Anthens, and Randolph H. Ware, 1992: GPS Meteorology: Remote Sensing of Atmospheric Water Vapor Using the Global Positioning System, Journal of Geophysical Research, Volume 97, pp. 15,787-15,801.

NASA WATER VAPOR PROJECT – MEaSUREs (NVAP-M), Algorithm Theoretical Basis Document, available on:
http://eosweb.larc.nasa.gov/sites/default/files/project/nvap/NVAP_M_ATBD_Feb2013.pdf

Niell, A. E., 1996: Global mapping functions for the atmosphere delay at radio wavelengths. Journal of Geophysical Research, Vol. 101, No. B2, pp. 3227–3246,

Niell, A. E., A. J. Coster, F. S. Solheim, V. B. Mendes, P. C. Toor, R. B. Langley, and C. A. Upham, 2001: Comparison of measurements of atmospheric wet delay by radiosonde, water vapor radiometer, GPS, and VLBI. J. Atmos. Oceanic Technol., Vol.18, 830– 850

Owens, J.C., 1967: Optical refractive index of air: Dependence on pressure, temperature and composition. Applied Optics, Vol.6, No.1,pp. 51-59

Paris, D. T., and F. K. Hurd, 1969: Basic Electromagnetic Theory. McGraw-Hill, New York.

Ruger,J.M, 2002: Refractive index formula for radio waves. FiG XXII International Congres, International Federation of Surveyors(FIG), Washington,D.C, April 19-26.

Saastamoinen, J., 1973: Contributions to the theory of atmospheric refraction. In three parts. Bulletin Geodesique, No.105, pp. 279-298; No.106, pp. 383-397; No.107, pp. 13-34.

Thayer, G. D. 1967: A rapid and accurate ray tracing algorithm for a horizontally stratified atmosphere. Radio Sci., Vol.2, No.1, pp. 249– 252.

Website1: http://eosweb.larc.nasa.gov/HORDERBIN/HTML_Start.cgi

Received: 2013-07-26,

Reviewed: 2013-11-19,

Accepted: 2013-19-20.